

# Entanglement transfer via Chiral Quantum Walk on a Triangular Chain

Utku Sağlam<sup>1,\*</sup> and Özgür E. Müstecaplıoğlu<sup>2,†</sup>

<sup>1</sup>*Department of Physics, 1150 University Avenue, University of Wisconsin at Madison, Madison, Wisconsin 53706, USA*

<sup>2</sup>*Department of Physics, Koç University, Sarıyer, İstanbul, 34450, Turkey*

(Dated: February 28, 2025)

We investigate the chiral quantum walk (CQW) for entanglement transfer on a triangular chain. We specifically consider two and three site Bell and W type entanglement cases, respectively. Using concurrence as quantum entanglement measure, together with the Bures distance and trace distance as the measures of the fidelity of the state transfer, we evaluate the success of the entanglement transfer. We compare the entangled state transfer time and quality in CQW against continuous-time quantum random walk. Furthermore, how the chain length and back-scattering at the end of the chain influence the entanglement transfer are pointed out.

## I. INTRODUCTION

Fast and accurate one-way transmission of quantum states through communication or computation networks is a critical objective for quantum technologies [1–3]. Proposed schemes to achieve this goal consider engineered couplings between the network sites [4–13], external fields [14–17], weak measurements [18, 19], or transport in noisy environments of biological or synthetic systems [20–24]. Such methods are challenging to implement in practice for profound quantum states, such as quantum entanglement transfer, due to quantum decoherence and disorder [25, 26]; besides they predict exponentially long transfer times with the channel length [27, 28]. Continuous time quantum walk (CTQW) is a paradigmatic model of quantum transport [29, 30]. Both discrete [31, 32] and continuous [33–36] time quantum walks have been discussed for perfect state transfer. CTQW can be made one-way by taking complex-valued couplings, which is called a chiral quantum walk (CQW) [37–39]. Chirality emerges due to breaking of time-reversal symmetry (TRS) [40], and it provides a significant boost to the transport speed [37].

The existence of high-dimensional entanglement is advantageous in quantum communication [41] and quantum superdense coding [42–44]. These multi-dimensional entangled states can be produced by repeatedly generating the entanglement in a low-dimensional system and transferring these to a higher dimensional one [45]. Our goal is to explore if CQW can be used to transmit two and three-dimensional quantum entangled states; what are the possible advantages it may offer regarding distance, speed, and transfer quality?

We specifically consider CQW on a linear chain of equilateral triangles, as shown in Fig. 1, which is the simplest graph that allows for so-called probability time symmetry (PTS) breaking [38]. A walker can transfer from one node to any other neighboring site on the triangular plaquette by passing through either one or two edges. We consider a uniform complex coupling between the nearest-neighbor sites. Due to the path length difference between odd and even number of edges traveled, and phases of the complex couplings, interference can enhance the transfer rate. For a triangular plaquette, the

maximum asymmetry in forward and backward time evolution is found when the phase of the couplings is  $\theta = \pi/2$  [38]. The system's initial state is taken to be an entangled state injected into the chain from the left. We consider two and three-site entanglement to explore the chiral transfer of both Bell and W class entangled states, which are significant for quantum communication and computation [46]. The quality of the transfer is examined by calculating the density matrix, concurrence [47], fidelity, Bures and trace distances explicitly [48–50]. Besides, we compared the time of transfer to characterize the speed-up advantage of CQW. The dependence of our results on the length of the chain has been discussed.

The triangular chain lattice can be realized in superconducting circuits [51, 52], trapped ions [53], NMR systems [38], photonic and spin waveguides [54], and in optical lattices [55]. In the case of optical lattices, complex edge weights could be introduced with the help of artificial gauge fields [56, 57] or with plasmonic non-Hermitian coupled waveguides [58].

This paper is organized as follows. We introduce the CQW on a triangular chain model by presenting the adjacency matrix and present the associated Hamiltonian model with complex hopping rates in Sec. II. Our results are given in Sec. III in five subsections. PTS breaking and entanglement transfer in CTQW and CQW on a triangular chain are discussed in Sec. III A and Sec. III B, respectively. Sec. III C describes how the entanglement transfer time and success scales with the chain length. The effects of backscattering on the entanglement transfer and the entanglement's long-time behavior are explained in Sec. III D. We end the results section by presenting the transfer of three-site entangled W states in Sec. III E. We conclude in Sec. IV.

## II. MODEL SYSTEM: CQW ON A TRIANGULAR CHAIN

We consider CQW on a triangular chain of  $N$  vortices as shown in Fig. 1. Triangular chain is a minimal graph where PTS can be broken [38] so that  $P_{nm}(t) \neq P_{mn}(t)$  or  $P_{nm}(t) \neq P_{nm}(-t)$ , where  $P_{nm}(t)$  ( $P_{nm}(-t)$ ) is the transition probability between the nodes  $n$  and  $m$  going forward (backward) in time. Breaking of PTS allows for enhanced quantum transport by CQW [37, 39].

We will use the site basis  $\{|i\rangle\}$ , with  $i = 1..N$  indicating which site is occupied such that  $|i\rangle := |0_1, 0_2, \dots, 1_i, \dots, 0_N\rangle$ .

\* Electronic address: [usaglam@wisc.edu](mailto:usaglam@wisc.edu)

† Electronic address: [omustecap@ku.edu.tr](mailto:omustecap@ku.edu.tr)

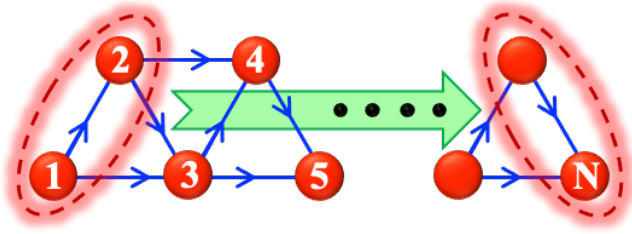


Figure 1. Graph of a linear chain of with  $N$  vortices arranged in triangular plaquettes. Initially, the pair of sites 1 and 2 at the left end of the chain are entangled. The entangled state is transported to the rightmost pair of vortices ( $N - 1$  and  $N$ ) after a chiral quantum walk. Arrows indicate the directed edges with complex weight factors, taken to be  $+i$ . In the opposite direction, the weight factors change phase and become  $-i$ . We have also examined transferring three-site entanglement from the leftmost plaquette (1, 2 and 3) to the right end of the chain.

Set of the coupled sites in a graph determine the edges  $e = (i, j)$ , which can be described by the so-called adjacency matrix  $A$  [59–62]. For a triangular chain of  $N = 5$  sites,  $A$  is given by

$$A = \begin{bmatrix} 0 & 1 & 1 & 0 & 0 \\ 1 & 0 & 1 & 1 & 0 \\ 1 & 1 & 0 & 1 & 1 \\ 0 & 1 & 1 & 0 & 1 \\ 0 & 0 & 1 & 1 & 0 \end{bmatrix}. \quad (1)$$

Together with the degree matrix  $D$  for the self edges ( $i, i$ ),  $A$ , determines the graph Laplacian  $L = D - A$ . Hamiltonian of the walk is given by the Hadamard product  $H = J \circ L$ , where  $J$  is the matrix of hopping rates (edge weights). We will take  $D = 0$  and write the Hamiltonian as

$$H = \sum_{nm} (J_{nm} A_{nm} |n\rangle\langle m| + J_{mn} A_{mn} |m\rangle\langle n|). \quad (2)$$

In contrast to CTQW where every  $J_{nm}$  is real-valued, CQW allows for complex edge weights, subject to  $J_{mn} = J_{nm}^*$ , so that the support graph of the walk becomes a directed one (cf. Fig. 1). Specifically, we take

$$H = \begin{bmatrix} 0 & -i & -i & 0 & 0 \\ i & 0 & -i & -i & 0 \\ i & i & 0 & -i & -i \\ 0 & i & i & 0 & -i \\ 0 & 0 & i & i & 0 \end{bmatrix} \quad (3)$$

The choice of the phase  $\theta_{nm} = \pi/2$  of complex hopping weights  $J_{nm} = |J_{nm}| \exp\{i\theta_{nm}\}$  (with  $n > m$ ) is based upon the general investigations of CQW [37] for a triangular plaquette. It is found that maximum bias in time asymmetry can be obtained at  $\theta = \pi/2$  [37]. We intuitively assume that a similar choice should yield efficient entanglement transfer along a linear chain of equilateral triangles, too. We numerically examined different choices and verified that our intuition is correct (Some typical results will be given in the results section, Sec. III).

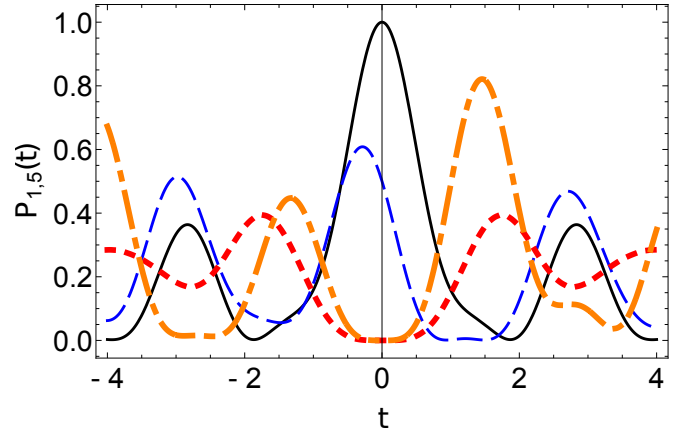


Figure 2. Time ( $t$ ) dependence of the occupation probabilities  $P_{1,5}(t)$  of sites 1 and 5 of a triangular chain with 5 sites, where a particle makes CTQW. For an initially localized particle with initial state  $|1\rangle$ ,  $P_1(t)$  and  $P_5(t)$  are indicated by black, solid and dashed, blue curves, respectively. For a particle initially in a quantum coherent superposition state  $|\psi(0)\rangle = (|1\rangle - \exp\{i\phi\}|2\rangle)/\sqrt{2}$  with  $\phi = 3\pi/4$ ,  $P_1(t)$  and  $P_5(t)$  are plotted by dot-dashed, orange and dotted, red curves, respectively.

$H$  determines the evolution of the initial state  $\rho(0)$  by  $\rho(t) = U\rho(0)U^\dagger$ , where  $U := \exp\{iHt\}$ . Initially, the leftmost pair of sites are entangled in a Bell state, and we aim to transfer the state to the right end of the chain. We will additionally consider an initial state in which three-sites of the leftmost triangular plaquette is entangled in a W-state.

Remarkably, CTQW, even with initial coherent superposition states on our linear triangular chain, could not yield perfect state transfer (PST) (cf. Fig. 2). The graphs that can support PST require to be hermitian, circulant, and to have distinct eigenvalues, together with a flat eigenbasis [35]. Alternatively, PST can still be achieved with a non-circulant graph that contains non-zero values on the certain off-diagonal elements of its adjacency matrix [36]. From a practical point of view, special graph structures for PST occupy a large volume with many qubits. Since our proposed adjacency matrix is neither circulant nor has required non-zero off-diagonal elements, we do not expect any PST. Our objective is to explore a chiral linear graph with more compact and practical unidirectional state transfer with high, albeit non-perfect efficiency.

### III. RESULTS

We will start with an examination of PTS-breaking in CTQW on the triangular chain as a benchmark of comparison with the results of CQW. We do not need complex edge weights to break PTS in general. The essential mechanism behind PTS breaking is the quantum path interference, for which the required phase difference, or quantum coherence, can be injected into the initial state instead of the edges. Specifically, we will consider a Bell-type entangled initial state

$$\psi(0) = \frac{1}{\sqrt{2}}(|1\rangle - e^{i\phi}|2\rangle) \quad (4)$$

on a regular triangular chain with real-valued hopping weights (We take  $J_{nm} = 1$  for simplicity).

Subsequently, we will investigate the transport of the initial entangled Bell state from the sites 1 and 2 to the sites 4 and 5 in CQW. We will compare the speed and concurrence of the transfer with the benchmark case of CTQW with the initial state in Eq. (4). Additionally, we analyze how the transfer speed and enhancement scale with the chain's length  $N$ , together with the long time behavior of the entanglement, which is non-trivial due to backscattering at the end of the chain. Finally, we consider a transfer of a W state,  $(|1\rangle + |2\rangle + |3\rangle)/\sqrt{3}$ , from the leftmost part to the rightmost part of the chain.

#### A. PTS breaking and entanglement transfer in CTQW on a triangular chain

To appreciate the role of the initial phase in Eq. (4) on the state transfer and PTS breaking in CTQW on the triangular chain, let's start with the initial state  $|\psi(0)\rangle = |1\rangle$ . The occupation probabilities  $P_i = \langle i|\rho(t)|i\rangle$  of the sites  $i = 1$  (solid, black) and  $i = 5$  (dashed, blue) are shown in Fig. 2, where mirror symmetry in the forward and backward going in time can be seen. Transfer from the initially occupied site  $|1\rangle$  to the rightmost site  $|5\rangle$  is found to be weak (less than 40% at any time).

If we use the initial state given in Eq. (4), in addition to be able to control path interference, PTS can be broken depending on the initial phase  $\phi$ . We have numerically compared  $P_5(t)$  for different  $\phi$  and found that  $\phi = 3\pi/4$  gives the largest occupation of site  $|5\rangle$ . Fig. 2 shows  $P_1(t)$  (dot-dashed, orange) and  $P_5(t)$  (dotted, red) for  $\phi = 3\pi/4$ , where time reversal asymmetry,  $P(t) \neq P(-t)$  emerges. Population transfer is significantly enhanced using such a quantum superposition state initially. We conclude that transferring a particle from left end of the chain to a site at the right end is more successful by injecting the particle simultaneously at two sites with a certain quantum coherence relative to starting a well localized particle at a single site. Let's now explore if similar advantages can be found in the entanglement transfer.

We can quantify the pairwise entanglement using the concurrence measure [47]. Concurrence for a state  $\rho$  is given by

$$C(\rho) = \max(0, \lambda_1 - \lambda_2 - \lambda_3 - \lambda_4), \quad (5)$$

where  $\lambda_i$ s, with  $i = 1..4$  and  $\lambda_{i+1} > \lambda_i$ , are the eigenvalues of  $R := (\rho^{1/2} \tilde{\rho} \rho^{1/2})^{1/2}$ . To calculate the concurrence  $C_{i,j}$  for the sites  $(i, j)$ , we first express the density matrix  $\rho(t)$  in the  $2^N$  dimensional basis of  $B := \{|0_1, \dots, 1_j, \dots, 0_N\rangle, j = 1..N\}$ . We then trace out the sites in the computational basis  $B$  other than  $i$  and  $j$  to find the reduced  $4 \times 4$  density matrix

$$\rho_{i,j}(t) = \text{Tr}_{\{B \setminus \{i,j\}\}}(\rho(t)), \quad (6)$$

for which  $C_{i,j}$  is easily evaluated.

Fig. 3 shows that the concurrence is optimum for  $\phi = \pm 3\pi/4$  with a value  $C_{4,5}(1.12) \sim 0.8$ . Therefore, for pairwise entanglement transfer,  $\phi = 3\pi/4$  gives the most advantageous initial

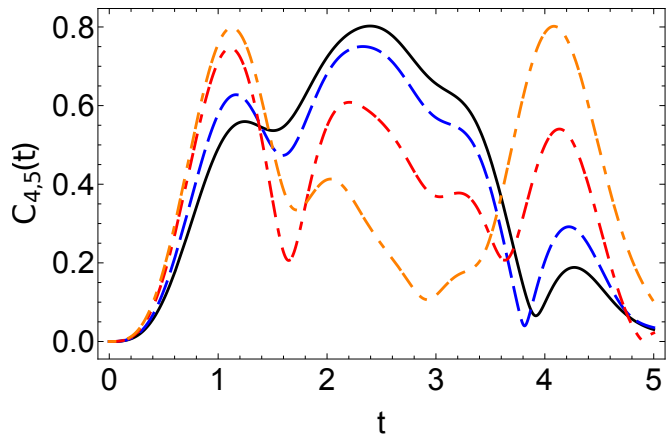


Figure 3. Time ( $t$ ) dependence of the concurrence  $C_{4,5}(t)$  to measure the entanglement between the sites  $|4\rangle$  and  $|5\rangle$  for an initially entangled state of the sites  $|1\rangle$  and  $|2\rangle$  of a particle that makes CTQW on a triangular chain of  $N = 5$  sites. Different curves stand for the initial states  $|\psi(0)\rangle = (|1\rangle - \exp\{i\phi\}|2\rangle)/\sqrt{2}$  with  $\phi = \pi/4$  (solid, black),  $\phi = \pm\pi/3$  (dashed, blue),  $\phi = \pm\pi/2$  (dot-dashed, orange),  $\phi = \pm 3\pi/4$  (dotted, red).

state. Remarkably, the same initial state yields the optimum population transfer (at a different time), too. A natural question to ask is if there is a fundamental connection of the critical phase  $\phi = 3\pi/4$  and PTS breaking in CTQW.

We can quantify the bias between the forward and backward time evolutions using the Bures distance between the states  $\rho(t)$  and  $\rho(-t)$ . Bures distance is defined by [48–50]

$$D_B(\rho, \sigma)^2 = 2(1 - \sqrt{F(\rho, \sigma)}), \quad (7)$$

where

$$F(\rho, \sigma) = [\text{Tr}(\sqrt{\sqrt{\rho}\sigma\sqrt{\rho}})]^2 \quad (8)$$

is the fidelity [63].

In Fig. 4 the Bures distance  $D_B$  is calculated for different  $\phi$ . For the phases 0 and  $\pm\pi$  the PTS is not broken and the Bures distance is zero. Largest bias in forward and backward time evolution is found for  $\phi = \pi/2$ , which is different than the critical phase  $\phi = 3\pi/4$  for optimum population and entanglement transfer in CTQW over triangular chain. We conclude that, instead of utilizing the broken-PTS, CTQW exploits the path interference for efficient state transfer.

#### B. PTS breaking and entanglement transfer in CQW on a triangular chain and comparison with CTQW

For CQW, we plot the concurrence in Fig. 5 by using an initial Bell state with  $\phi = \pi$  in Eq. (4) and different  $\theta$  in Eq. (3). We see that the concurrence is largest for  $\theta = \pi/2$  with a value  $C_{4,5}(1.02) \sim 0.9$ , indicating that CQW has a slight time advantage ( $\Delta t \sim 0.1$ ) along with a significantly higher quality transfer of entanglement compared to CTQW (cf. Fig. 3). Without plotting, we state here that similar conclusion is applicable to occupation probabilities, too. We found that CQW

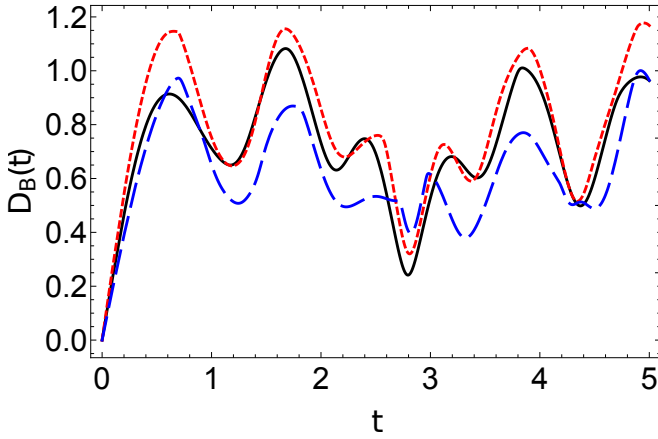


Figure 4. Time ( $t$ ) dependence of the Bures distance between the forward and backward evolved density matrices  $\rho(t)$  and  $\rho(-t)$ , for a CTQW on a triangular chain. The curves are for the coherence phases  $\phi$  in the initial state  $|\psi(0)\rangle = (|1\rangle - \exp\{i\phi\}|2\rangle)/\sqrt{2}$  with  $\phi = \pm\pi/3$  (dashed, blue),  $\phi = \pm\pi/2$  (dot-dashed, orange), and  $\phi = \pm 3\pi/4$  (dotted, red). The Bures distance for the phases  $\phi = 0$  and  $\phi = \pm\pi$  are zero.

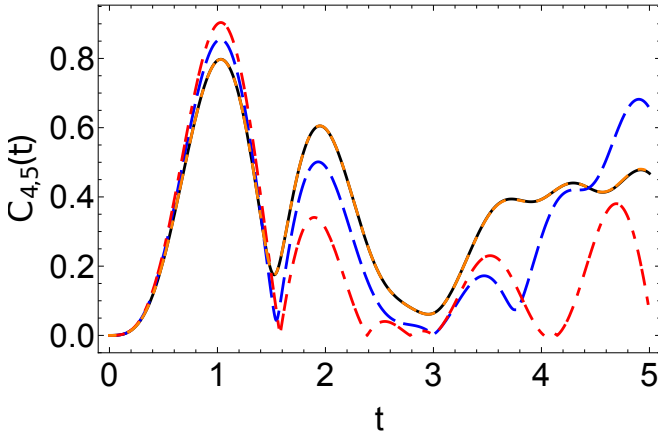


Figure 5. Time ( $t$ ) dependence of the concurrence  $C_{4,5}$  measuring the pairwise entanglement between the sites  $|4\rangle$  and  $|5\rangle$  of a triangular chain of  $N = 5$  sites over which an initial maximally entangled Bell state  $(|1\rangle + |2\rangle)/\sqrt{2}$  of the sites 1 and 2 undergoes CQW. Different curves are for the different complex hopping coefficients of the CQW with the phases  $\theta = \pi/4$  (solid, black),  $\theta = \pm\pi/3$  (dashed, blue),  $\theta = \pm\pi/2$  (dot-dashed, orange),  $\theta = \pm 3\pi/4$  (dotted red).

with  $\theta = \pi/2$  yields near perfect ( $P_5 \sim 0.95$ ) state transfer  $|1\rangle \rightarrow |5\rangle$  at  $t \sim 1.64$ .

We calculated the concurrences for  $\phi = \pi/4$ ,  $\phi = \pi/3$ ,  $\phi = \pi/2$ ,  $\phi = 3\pi/4$  and looked for the optimum  $\theta$  values. We have found that for the maximally entangled ( $\phi = \pi$ ) initial Bell state,  $\theta = \pi/2$  gives the optimum (maximum) concurrence  $C_{4,5}(1.02) \sim 0.9$ .

We plot the Bures distance  $D_B(t)$  in Fig. 6, which shows that  $D_B(t)$  is maximum for  $\theta = \pm\pi/2$  (dot-dashed, orange). Remarkably, maximum broken PTS in the CTQW is found for  $\phi = \pi/2$ . This suggests that  $\phi = \theta = \pm\pi/2$  is an optimal choice for the broken-PTS condition both for CTQW and

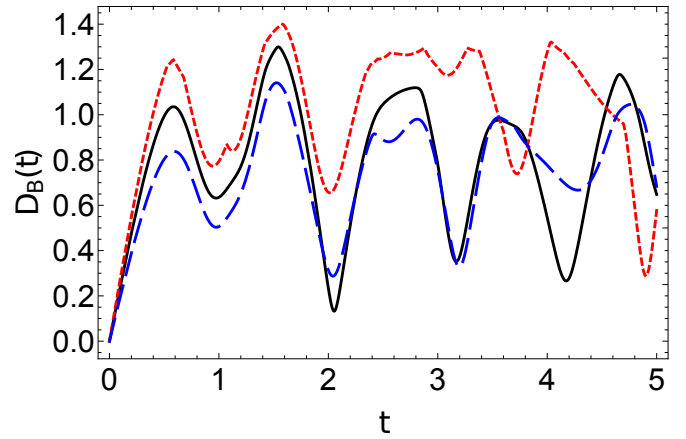


Figure 6. Time ( $t$ ) dependence of the Bures distance  $D_B(t)$  between the forward and backward evolved density matrices  $\rho(t)$  and  $\rho(-t)$ , respectively, for a CQW on a triangular chain of  $N = 5$  sites. Initially the quantum walker is in a maximally entangled Bell state  $(|1\rangle + |2\rangle)/\sqrt{2}$ . Different curves are for chains with different complex hopping coefficients of phases  $\theta = \pm\pi/3$  (dashed, blue),  $\theta = \pm\pi/2$  (dot-dashed, orange) and  $\theta = \pm 3\pi/4$  (dotted, red). The Bures distance for the phases  $\theta = 0$  and  $\pm\pi$  are zero; and for  $\theta = \pi/4$   $D_B(t)$  is the same as that of  $\theta = 3\pi/4$ .

CQW over a triangular chain. Critical angle of maximum time reversal asymmetry however coincides with critical angle of optimum state transfer only for the CQW.

In Fig. 7, the concurrences for CQW and CTQW with an initial state of  $(|1\rangle + |2\rangle)/\sqrt{2}$  are plotted. Solid red curve represents the CQW case and dashed blue line is for the CTQW case. This plot also demonstrates the broken-PTS in the CQW case. Here, one can notice the relatively higher entanglement transfer quality in CQW. In addition, the transfer time is relatively shorter in the case of CQW by  $\Delta t \sim 0.4$ .

To demonstrate the uni-directionality of the entanglement transfer, we plot the dynamics of the concurrences  $C_{i,j}$  that measure entanglement between every pair of sites  $(i, j)$  of the triangular chain in Fig 8. One can see that the unidirectional transfer of entanglement from the sites  $(|1\rangle, |2\rangle)$  towards the sites  $(|4\rangle, |5\rangle)$  propagates from left to right by passing through the intermediate sites as  $(|1\rangle, |2\rangle) \rightarrow (|2\rangle, |3\rangle) \rightarrow (|2\rangle, |4\rangle) \rightarrow (|3\rangle, |4\rangle) \rightarrow (|4\rangle, |5\rangle)$ .

### C. Scaling of Entanglement Transfer with the Chain Length

For long chains with large  $N$ 's, the concurrence calculation became computationally demanding. Therefore, in this section, we utilize the Trace Distance [63] measure to characterize the quality of the state transfer. Furthermore, to simplify the calculations, we will take two 2 sub-matrices (9) and (10) out of the full density matrix of the chain such that

$$S_i(0) = \begin{bmatrix} \rho_{1,1}(0) & \rho_{1,2}(0) \\ \rho_{2,1}(0) & \rho_{2,2}(0) \end{bmatrix}, \quad (9)$$

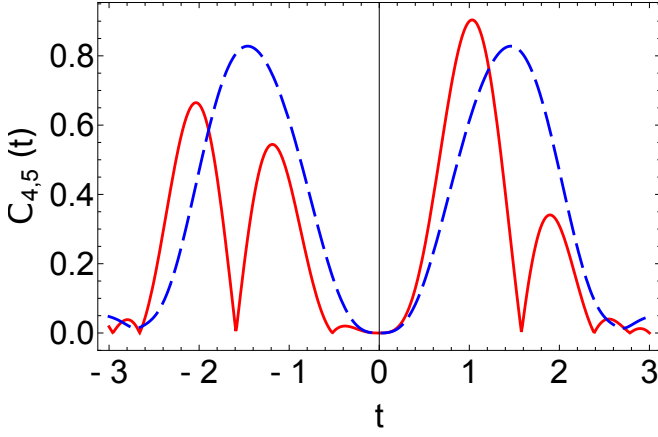


Figure 7. Time( $t$ ) dependence of the concurrence  $C_{4,5}(t)$  to measure the entanglement between the sites  $|4\rangle$  and  $|5\rangle$  for an initially maximally entangled Bell state  $(|1\rangle + |2\rangle)/\sqrt{2}$  of the sites  $|1\rangle$  and  $|2\rangle$  of a particle that makes CTQW (dashed, blue) and CQW (solid, red) with  $\theta = \pi/2$  on a triangular chain of  $N = 5$  sites. We take the phases of the complex hopping coefficients as  $\theta = \pi/2$  for CQW; while for CTQW hopping coefficients are real with  $\theta = 0$ .

and

$$S_f(t) = \begin{bmatrix} \rho_{4,4}(t) & \rho_{4,5}(t) \\ \rho_{5,4}(t) & \rho_{5,5}(t) \end{bmatrix}. \quad (10)$$

The trace distance ( $TD$ ) is then evaluated by [63]

$$TD(t) = \frac{1}{2} \text{Tr} |S_f(t) - S_i(t)|, \quad (11)$$

where  $|X| \equiv (X^\dagger X)$  is the positive square root of  $X^\dagger X$ . The full density matrix initially consists of zeros in other elements. For the initial states that we consider here,  $S_i(0)$  is a faithful representation of the full density matrix of interest. After the quantum walk, if the state transfer is successful, the significant elements of the final density matrix should be close to that of  $S_i(0)$ , and hence we limit ourselves to the comparison of  $S_f(t)$  and  $S_i(0)$  elements instead of the full density matrices. This approach brings significant computational advantage and captures the essential physics.

In addition, since the PTS is broken on odd-numbered cycles during CQW [38], we only consider triangular chains with odd number of vortices during the computation of the entanglement transfer behaviour with respect to the chain size  $N$ .

When TD reaches to a local minimum, one can argue that the state transfer is complete. Aiming to demonstrate the quality and speed of a maximally entangled state transfer with  $\theta = \pi/2$  and  $\phi = \pi$ , we calculate the time when the first local minimum of TD happens for each odd  $N$  and identify it as the shortest time for the state transfer, denoted by  $T_{\min}$ . Our results are plotted in Fig. 9a. Typically, in simple uniform one-dimensional spin chains, state transfer time scales up exponentially with the length of the chain [27, 28]. In contrast, Fig. 9a reveals that state transfer time in both CQW and CTQW on a triangular chain grows linearly with the chain length represented by the number of vertices. CQW can be seen to be the faster medium

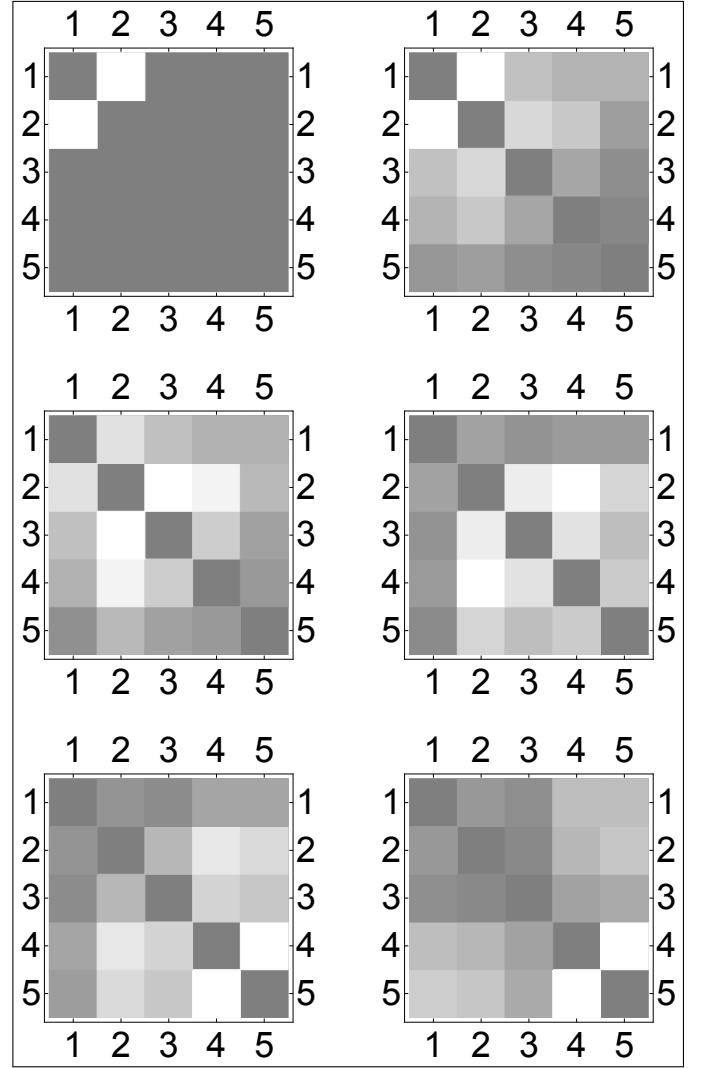


Figure 8. The time ( $t$ ) evolution of concurrence  $C_{i,j}$ , measuring the pairwise entanglement between the sites  $|i\rangle$  and  $|j\rangle$ , is shown as a matrix with  $i, j = 1..5$ . Colors from light to dark scale with 1 to 0, respectively. Initially (at  $t = 0$ ), the quantum walker is injected in the maximally entangled Bell state of the sites 1 and 2 with  $C_{1,2} = 1$  (upperleft panel) to undergo CQW with complex hopping coefficients with phase  $\theta = \pi/2$ . As the time progresses, one can notice the unidirectional transfer of entanglement (light colored pair of squares) to the rightmost sites 4 and 5. The panels are for the  $t = 0$  (upper left),  $t = 0.2$  (upper right),  $t = 0.4$  (middle left),  $t = 0.6$  (middle right),  $t = 0.8$  (bottom left), and  $t = 1$  (bottom right).

of state transfer relative to CTQW. The short state transfer time advantage of CQW over CTQW is more prominent for longer chain lengths.

In addition to the speed, quality of the state transfer in CQW and CTQW should be compared. For that aim, Fig. 9b plots the TD for CQW and CTQW with respect to odd  $N$ . TD in CTQW is not close to zero and hence the quality for the state transfer is very low. On the other hand, CQW displays highly successful state transfer for small  $N$ . State transfer quality in CQW becomes poor for chains longer than  $N \sim 11$  sites. In

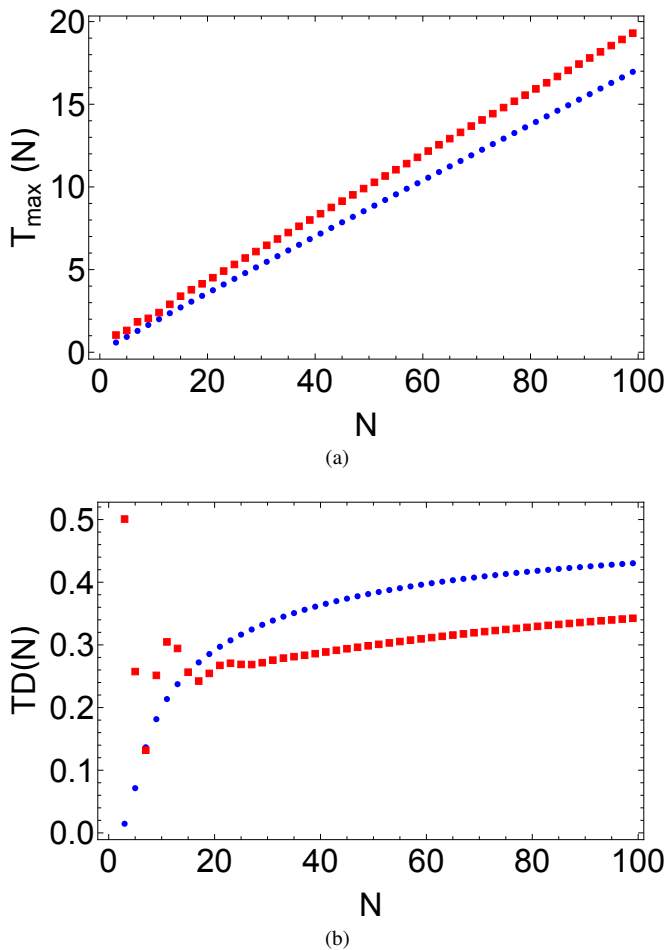


Figure 9. (a) Shortest state transfer time  $T_{\min}$  for CQW (circle, blue) and CTQW (square, red) on a triangular chain of odd number of  $N$  sites. (b) Trace distance  $TD$  between  $S_i(0)$  and  $S_f(t)$  (effective initial and final states) with respect to  $N$  for CQW (circle, blue) and CTQW (square, red). Initial state is a Bell state  $(|1\rangle + |2\rangle)/\sqrt{2}$  of the leftmost sites 1 and 2. Final state is the state at time  $t$  when the  $TD$  becomes the first local minimum. The phase of the complex edge weights is taken to be the optimal value of  $\theta = \pi/2$ .

chains of different  $N$ 's, transferring a state with a given  $\phi$  can be optimized by selecting a critical phase  $\theta$  of the complex edge weights of the triangular chain. For chains shorter than  $N \sim 11$ , we find that  $\theta = \pi/2$  is the most efficient one. For simplicity, we fix  $\theta = \pi/2$  in Figs. 9a and 9b, instead of using a different  $\theta$  for each  $N$ .

Dynamics of  $TD$  for  $N = 3, 5, 7$  is shown in Fig. 10. First local minima of  $TD$  emerges when the state reaches the end of the chain. For  $N = 3$  near perfect state transfer is possible. For longer chains, quality of the transfer gets progressively worse. A surprising observation is the revivals of the state transfer for  $N = 3$ . A question can then be asked if longer chains can also give revivals and better success if we sacrifice unidirectional evolution and allow backscattering at the end of the chain.

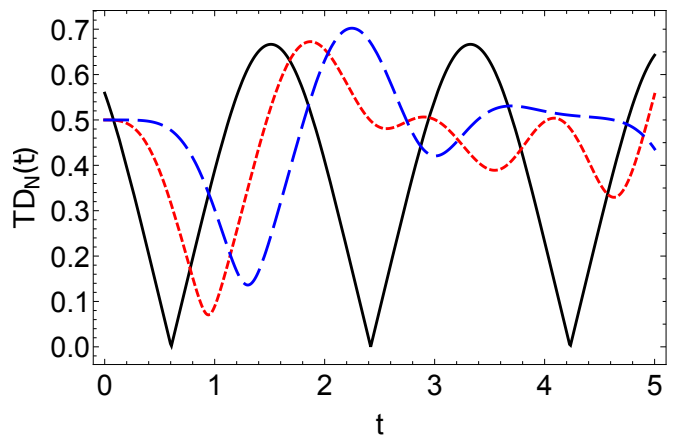


Figure 10. Time  $t$  dependence of the trace distance  $TD$  between  $S_i(0)$  and  $S_f(t)$  (effective initial and final states) for triangular chains of  $N = 3$  (solid, black),  $N = 5$  (dashed, blue), and  $N = 7$  (dot-dashed, red) sites. Initial state is a Bell state  $(|1\rangle + |2\rangle)/\sqrt{2}$  of the leftmost sites 1 and 2. Final state is the state at time  $t$  when the  $TD$  becomes the first local minimum. The phase of the complex edge weights is taken to be the optimal value of  $\theta = \pi/2$ .

#### D. Long-term Behaviour of the Entanglement Transfer on Triangular Chain

So far, we have focused on the unidirectional transfer of states from the left to the right ends of the triangular chain. On the other hand, Figs. 2-7 and Fig. 10 indicate an oscillatory behavior in the quality of state transfer, which arises due to the scattering of the quantum walker from the end of the chains. These oscillations yield either periodic or decreasing changes in the concurrence, occupation probability, trace distance, and Bures distance. Accordingly, ideally, it can be assumed that the state has been measured or collected by a sink (terminal lead) at the end of the chain in practice. The decrease of the transfer quality after backscattering can be compared with the well-known collapse phenomenon of a wave with multiple frequencies due to destructive interference, or noise, leading to loss of wave coherence. Here, instead of frequency, we have path length-dependent phase factors, which are further controlled by the initial coherence phase  $\phi$  and the phase of the complex hopping factors  $\theta$ . For short times, the quantum walker will only be able to develop several different phases, and hence they will act as a decoherent noise with a destructive interference effect. However, due to the finite chain and discrete nature of the phases the system can support, the walker could eventually build the same phases that can constructively interfere if we let the walker move for a sufficiently long time. Hence, we can predict the initial state can revive significantly for a near-perfect transfer in long-time evolution.

Using  $\phi = \pi$  and  $\theta = \pi/2$ , we calculate the trace distance between  $S_i(t)$  and  $S_f(t)$  over a more extended range of time for a triangular chain of  $N = 5$  sites, and the result is plotted in Fig. 11. We see that a chaotic looking interference pattern emerges due to multiple phase differences developing in the long-term evolution. However, the system's discrete and finite nature gives a finite set of phases, which leads to constructive

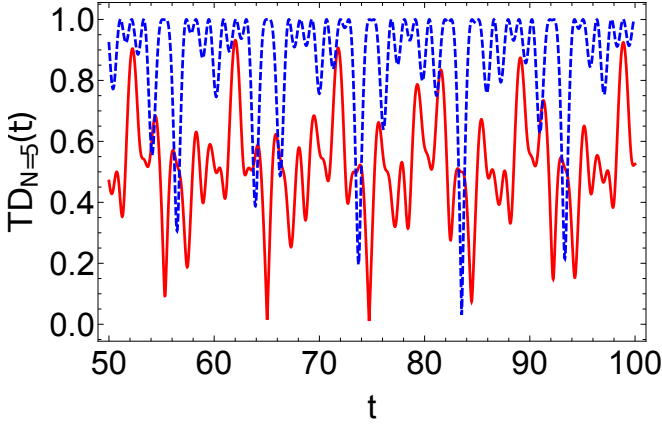


Figure 11. Trace distance ( $TD$ ) between forward  $\rho(t)$  and backward  $\rho(-t)$  evolved states as a function of time  $t$  (dotted, blue). Initial state is a Bell state  $(|1\rangle + |2\rangle)/\sqrt{2}$  of the leftmost sites 1 and 2 and subject to CQW on a triangular chain of  $N = 5$  sites. The chain has complex edge weights with the same phases  $\theta = \pi/2$ . Trace distance between the initial state and the reduced state of the last pair of sites 4, 5 is also plotted (solid, red).

interference at some instants. We find near-perfect transfer around  $t \sim 65$  and  $t \sim 75$ , in contrast to poor state transfer quality at the time of the first local minimum of the  $TD$ . Fig. 11 shows the  $TD$  between  $\rho(t)$  and  $\rho(-t)$  as well. A remarkable similarity between the dynamics of PTS breaking and state transfer quality can be noticed. At  $t \sim 75$ , where we have near-perfect state transfer, PTS breaking is also almost perfect with the associated  $TD \sim 0.9995$ .

In practice, the benefits of long-time revived near-perfect state transfer may be limited by the environmental effects where the quantum walk is implemented. We did not consider the quantum decoherence and dephasing effects of the environment here. Open system dynamics should be used with mixed states in order to answer this question for a given physical system with properly identified quantum decoherence channels specific to physical implementation.

### E. Transfer of W states in CQW along a triangular chain

We address the scalability of state transfer by CQW on a triangular chain of  $N$  sites by considering an initial W-state,  $(|1\rangle + |2\rangle + |3\rangle)/\sqrt{3}$ . To assess the quality of the W-state transfer, we calculate the Bures Distance between the initial W state on 1st, 2nd, and 3rd sites:  $\rho_{1,2,3}(0)$ , and the final state on 3rd, 4th, and 5th sites:  $\sigma_{3,4,5}(t)$  using

$$\rho_{1,2,3}(0) = Tr_{4,5}(\rho(0)), \quad \sigma_{3,4,5}(t) = Tr_{1,2}(\rho(t));$$

$$D_B(t) := 2 \left( 1 - \sqrt{F(\rho_{1,2,3}(0), \sigma_{3,4,5}(t))} \right). \quad (12)$$

Fig. 12 shows that  $D_B(t)$  reaches to a minimum value  $D_B(t) \sim 0.2$  at  $t \sim 0.6$  and  $t \sim 1.6$ . We conclude that transfer of W state is less successful than transfer of Bell state in short-time unidirectional transfer regime. We find a similar

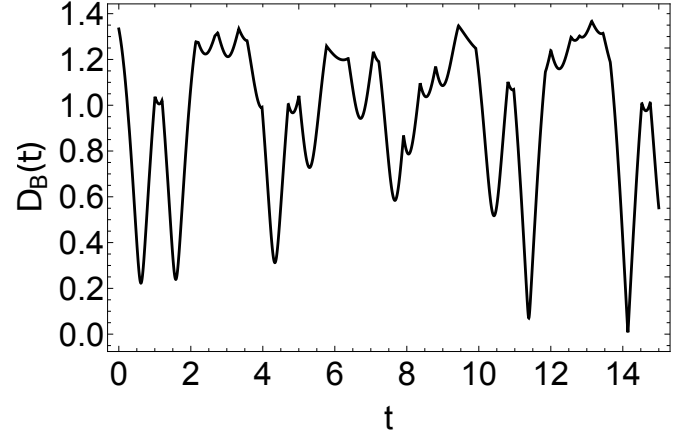


Figure 12. Time ( $t$ ) dependence of the Bures distance between initial  $\rho_{1,2,3}(0)$  and final  $\sigma_{3,4,5}(t)$  as a function of time  $t$  with an initial W-state  $(|1\rangle + |2\rangle + |3\rangle)/\sqrt{3}$  under the scheme of CQW on a triangular chain of  $N = 5$  sites with complex edge weights of phase  $\theta = \pi/2$ .

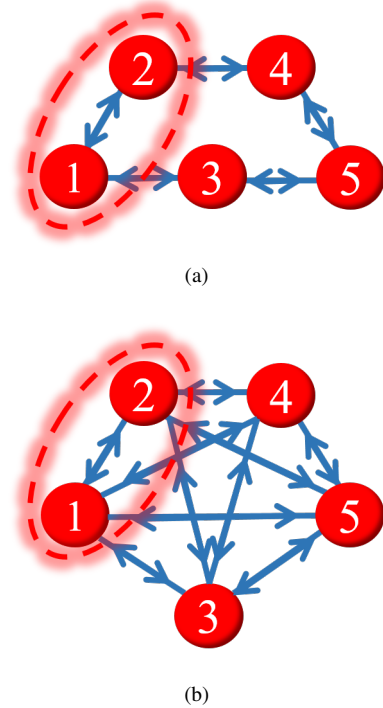


Figure 13. (a) Graph of a linear chain of 5 vortices arranged as an odd number cycle. (b) Graph of a linear chain of 5 vortices arranged as a hexagon with five pointed star-like diagonal connections.

quality transfer of the W-state over a longer triangular chain of  $N = 7$  sites. Similar to the Bell state transfer, W state transfer exhibits revival oscillations, which can be exploited for more efficient transfer. When the long-term revival oscillations considered in a  $5 \times 5$  triangular chain graph, revival oscillations cause the trace distance to fall to a value of  $TD(t) \sim 0$  at time  $t \sim 14.1$ . Which implies an improved transfer quality compared to the short-time transfer regimes.

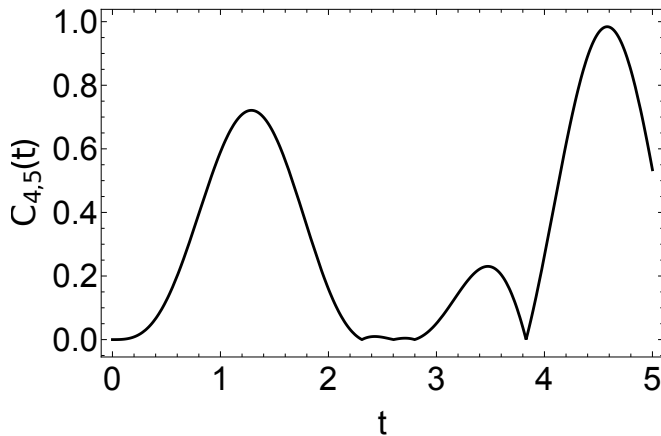


Figure 14. Time( $t$ ) dependence of the concurrence  $C_{4,5}(t)$  to measure the entanglement between the sites  $|4\rangle$  and  $|5\rangle$  on a  $5 \times 5$  circulant graph with only nearest-neighbour interactions for an initially maximally entangled Bell state  $(|1\rangle + |2\rangle)/\sqrt{2}$  of the sites  $|1\rangle$  and  $|2\rangle$  of a particle that makes CTQW.

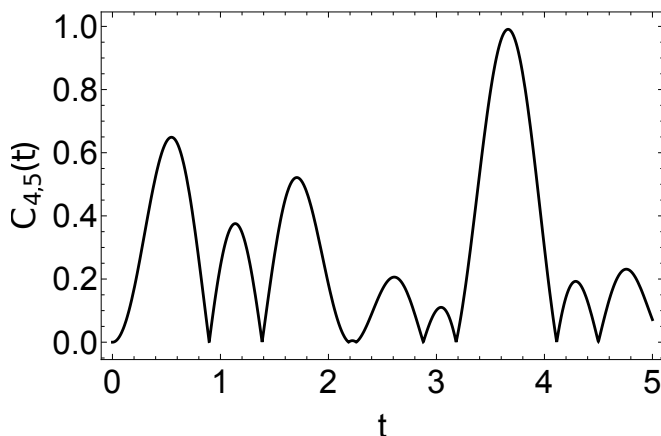


Figure 15. Time( $t$ ) dependence of the concurrence  $C_{4,5}(t)$  to measure the entanglement between the sites  $|4\rangle$  and  $|5\rangle$  on a complete hexagonal graph for an initially maximally entangled Bell state  $(|1\rangle + |2\rangle)/\sqrt{2}$  of the sites  $|1\rangle$  and  $|2\rangle$  of a particle that makes CTQW.

#### IV. CONCLUSION

We explored the transfer of spatial entanglement of a single particle undergoing CQW on a triangular chain. To appreciate the advantages of CQW, we first considered the case of CTQW. We found that particle transfer to the end of the chain is more successful if the particle is injected simultaneously from the leftmost pair of sites in a specific quantum (Bell-type) superposition state. The success, measured by the rightmost site's occupation probability, depends on the phase  $\phi$  of the initial quantum coherent superposition. For the same  $\phi$ , but at a different time, transfer of the entire state, which is a maximally entangled state, is also the most successful. Using the Bures distance between the forward and backward time evolved states, we examined the dynamics of PTS breaking at different  $\phi$ . Though CTQW can break the PTS at certain  $\phi$ , these phases

are not critical for an optimal state transfer. The essential mechanism behind the quality of state transfer via CTQW is path interference.

Similar investigations for the CQW revealed that CQW is superior to CTQW in population and entanglement transfers efficiency while the speeds are comparable for short chains, confirming the previous results [37, 38]. Calculating the trace distance and Bures distance, we justified that CQW exploits broken PTS to further enhance the state transfer quality. Remarkably, using the phase  $\theta$  of the complex edge weights in CQW, the state transfer's success for different  $\phi$  can be optimized, which is not possible with CTQW. For longer chains, the speed advantage in CQW is more prominent.

In contrast to the exponential growth of PST time in one-dimensional spin chains [27, 28, 35, 36], a triangular chain allows for linear scaling of the transfer speeds in CTQW and CQW. However, the transfer's fidelity severely reduces if we limit ourselves with the unidirectional evolution along the chain. For longer times, strong revivals of the state at the end of the chain emerges so that almost perfect state transfer becomes possible even for longer chains. Fidelity of transfer reduces relative to that of Bell state transfer if we aim to transfer a W state with tripartite spatial entanglement unidirectionally; on the other hand, nearly perfect W state transfer is possible in the long-time regime.

Our results can be significant fundamentally to illuminate the interplay of PTS breaking and entanglement transfer, and practically to design optimum chiral lattices for long-distance transfer of multipartite entangled states in physical platforms such as plasmonic non-Hermitian coupled waveguides [58], ultracold atomic optical lattices [55], photonic-spin waveguides [54], or quantum superconducting circuits [51, 52].

#### V. ACKNOWLEDGEMENTS

The authors thank Deniz N. Bozkurt for fruitful discussions.

#### Appendix: Perfect state and entanglement transfer on a circulant graphs

We present perfect state and entanglement transfer on some circulant graphs in this appendix. Such graphs occupy a relatively large space than linear triangular chains to transfer a state over the same distance and require more qubits to implement. For example, we take a  $5 \times 5$  circulant graph shown in Fig.13a with only nearest-neighbor interactions. The adjacency matrix for such a graph is

$$A = \begin{bmatrix} 0 & -i & -i & 0 & 0 \\ i & 0 & 0 & -i & 0 \\ i & 0 & 0 & 0 & -i \\ 0 & i & 0 & 0 & -i \\ 0 & 0 & i & i & 0 \end{bmatrix}. \quad (\text{A.1})$$

Fig. 14 shows that the entanglement transfer on such a graph is nearly perfect with a concurrence of  $C \sim 0.98$  at  $t \sim 4.6$ .

Another example is a hexagonal graph with diagonal connections which is sketched on Fig.13b. This graph contains three triangular plaquettes, but being circulant comes with the

cost of more edges. The adjacency matrix reads

$$A = \begin{bmatrix} 0 & -i & -i & -i & i \\ i & 0 & -i & -i & -i \\ i & i & 0 & -i & -i \\ i & i & i & 0 & -i \\ i & i & i & i & 0 \end{bmatrix}. \quad (\text{A.2})$$

Fig. 15 presents the possibility of nearly perfect entanglement transfer with a concurrence of  $C_{4,5} \sim 1$  at  $t \sim 3.7$ .

- 
- [1] C. H. Bennett and D. P. DiVincenzo, *Nature* **404**, 247 (2000).  
[2] D. P. DiVincenzo, *Fortschritte der Phys.* **48**, 771 (2000).  
[3] H. J. Kimble, *Nature* **453**, 1023 (2008).  
[4] S. Bose, *Phys. Rev. Lett.* **91**, 207901 (2003).  
[5] M. Christandl, N. Datta, A. Ekert, and A. J. Landahl, *Phys. Rev. Lett.* **92**, 187902 (2004).  
[6] C. Albanese, M. Christandl, N. Datta, and A. Ekert, *Phys. Rev. Lett.* **93**, 230502 (2004).  
[7] A. Wójcik, T. Łuczak, P. Kurzyński, A. Grudka, T. Gdala, and M. Bednarska, *Phys. Rev. A* **72**, 034303 (2005).  
[8] C. Di Franco, M. Paternostro, and M. S. Kim, *Phys. Rev. Lett.* **101**, 230502 (2008).  
[9] M. Mohseni, P. Rebentrost, S. Lloyd, and A. Aspuru-Guzik, *J. Chem. Phys.* **129**, 174106 (2008).  
[10] T. J. G. Apollaro, L. Banchi, A. Cuccoli, R. Vaia, and P. Verrucchi, *Phys. Rev. A* **85**, 052319 (2012).  
[11] I. Sinayskiy, A. Marais, F. Petruccione, and A. Ekert, *Phys. Rev. Lett.* **108**, 020602 (2012).  
[12] K. Korzekwa, P. Machnikowski, and P. Horodecki, *Phys. Rev. A* **89**, 062301 (2014).  
[13] M. P. Estarellas, I. D'Amico, and T. P. Spiller, *Phys. Rev. A* **95**, 042335 (2017).  
[14] T. Shi, Y. Li, Z. Song, and C.-P. Sun, *Phys. Rev. A* **71**, 032309 (2005).  
[15] M. J. Hartmann, M. E. Reuter, and M. B. Plenio, *New J. Phys.* **8**, 94 (2006).  
[16] L. Banchi, T. J. G. Apollaro, A. Cuccoli, R. Vaia, and P. Verrucchi, *Phys. Rev. A* **82**, 052321 (2010).  
[17] H. J. Shan, C. M. Dai, H. Z. Shen, and X. X. Yi, *Sci. Rep* **8**, 13565 (2018).  
[18] Z. He, C. Yao, and J. Zou, *Phys. Rev. A* **88**, 044304 (2013).  
[19] Z.-X. Man, N. B. An, Y.-J. Xia, and J. Kim, *Phys. Lett. A* **378**, 2063 (2014).  
[20] A. Zwick, G. A. Álvarez, G. Bensusky, and G. Kurizki, *New J. Phys.* **16**, 065021 (2014).  
[21] D.-X. Li, D.-X. Li, X.-M. Liao, X.-M. Liao, X.-Q. Shao, and X.-Q. Shao, *Opt. Express* **27**, 35971 (2019).  
[22] Y. Matsuzaki, V. M. Bastidas, Y. Takeuchi, W. J. Munro, and S. Saito, *J. Phys. Soc. Japan* **89**, 044003 (2020).  
[23] R. Vieira and G. Rigolin, *Phys. Lett. A* **384**, 126536 (2020).  
[24] W.-K. Mok, D. Aghamalyan, J.-B. You, T. Haug, W. Zhang, C. E. Png, and L.-C. Kwek, *Phys. Rev. Res.* **2**, 013369 (2020).  
[25] G. De Chiara, D. Rossini, S. Montangero, and R. Fazio, *Phys. Rev. A* **72**, 012323 (2005).  
[26] S. Ashhab, *Phys. Rev. A* **92**, 062305 (2015).  
[27] X. Chen, R. Mereau, and D. L. Feder, *Phys. Rev. A* **93**, 012343 (2016).  
[28] R. Sousa and Y. Omar, *New J. Phys.* **16**, 123003 (2014).  
[29] O. Mülken and A. Blumen, *Phys. Rep.* **502**, 37 (2011).  
[30] A. Ambainis, *Int. J. Quantum Inf.* **01**, 507 (2003).  
[31] X. Zhan, H. Qin, Z.-h. Bian, J. Li, and P. Xue, *Phys. Rev. A* **90**, 012331 (2014).  
[32] M. Štefaňák and S. Skoupý, *Phys. Rev. A* **94**, 022301 (2016).  
[33] V. M. Kendon and C. Tamon, *J. Comput. Theor. Nanosci.* **8**, 422 (2011).  
[34] S. J. Large, M. S. Underwood, and D. L. Feder, *Phys. Rev. A* **91**, 032319 (2015).  
[35] S. Cameron, S. Fehrenbach, L. Granger, O. Hennigh, S. Shrestha, and C. Tamon, *Linear Algebra Appl.* **455**, 115 (2014).  
[36] E. Connelly, N. Grammel, M. Kraut, L. Serazo, and C. Tamon, *Linear Algebra Appl.* **531**, 516 (2017).  
[37] Z. Zimborás, M. Faccin, Z. Kádár, J. D. Whitfield, B. P. Lanyon, and J. Biamonte, *Sci. Rep* **3** (2013).  
[38] D. Lu, J. D. Biamonte, J. Li, H. Li, T. H. Johnson, V. Bergholm, M. Faccin, Z. Zimborás, R. Laflamme, J. Baugh, and S. Lloyd, *Phys. Rev. A* **93**, 042302 (2016).  
[39] T. G. Wong, *J. Phys. A Math. Theor.* **48**, 405303 (2015).  
[40] Y. Liu and D. L. Zhou, *Phys. Rev. A* **91**, 052318 (2015).  
[41] D. Cozzolino, B. D. Lio, D. Bacco, and L. K. Oxenløwe, *Adv. Quantum Technol.* **2**, 1900038 (2019).  
[42] X. S. Liu, G. L. Long, D. M. Tong, and F. Li, *Phys. Rev. A* **65** (2002).  
[43] A. Grudka and A. Wójcik, *Phys. Rev. A* **66** (2002).  
[44] X. M. Hu, Y. Guo, B. H. Liu, Y. F. Huang, C. F. Li, and G. C. Guo, *Sci. Adv.* **4**, 10.1126/sciadv.aat9304 (2018).  
[45] T. Giordani, L. Innocenti, A. Suprano, E. Polino, M. Paternostro, N. Spagnolo, F. Sciarrino, and A. Ferraro, *arXiv:2010.07127*.  
[46] W. Dür, G. Vidal, and J. I. Cirac, *Phys. Rev. A* **62**, 062314 (2000).  
[47] W. K. Wootters, *Phys. Rev. Lett.* **80**, 2245 (1998).  
[48] R. Jozsa, *J. Mod. Opt.* **41**, 2315 (1994).  
[49] M. Hübner, *Phys. Lett. A* **163**, 239 (1992).  
[50] M. Hübner, *Phys. Lett. A* **179**, 226 (1993).  
[51] A. Vepsäläinen and G. S. Paraoanu, *Adv. Quantum Technol.* **3**, 1900121 (2020).  
[52] K. K. W. Ma, *Phys. Rev. A* **102** (2020).  
[53] T. Manovitz, Y. Shapira, N. Akerman, A. Stern, and R. Ozeri, *PRX Quantum* **1**, 020303 (2020).  
[54] T. Ramos, B. Vermersch, P. Hauke, H. Pichler, and P. Zoller, *Phys. Rev. A* **93**, 062104 (2016).  
[55] J. K. Pachos and M. B. Plenio, *Phys. Rev. Lett.* **93**, 056402 (2004).  
[56] I. Bloch, J. Dalibard, and W. Zwerger, *Rev. Mod. Phys.* **80**, 885 (2008).  
[57] M. Aïdelsburger, S. Nascimbene, and N. Goldman, *CR PHYS* **19**, 394 (2018).

- [58] Z. Fu, N. Fu, H. Zhang, Z. Wang, D. Zhao, and S. Ke, *Appl. Sci.* **10**, 3425 (2020).
- [59] J. Kempe, *Contemp. Phys.* **44**, 307 (2003).
- [60] A. Sett, H. Pan, P. E. Falloon, and J. B. Wang, *Quantum Inf. Process.* **18** (2019).
- [61] E. Farhi and S. Gutmann, *Phys. Rev. A* **58**, 915 (1998).
- [62] A. M. Childs, E. Farhi, and S. Gutmann, *Quantum Inf. Process.* **1**, 35 (2002).
- [63] I. L. C. Michael A. Nielsen, *Quantum Computation and Quantum Information* (Cambridge University Press, Cambridge, 2010).